Featuring work from Technion - Israel Institute of Technology (Moran Bercovici) & IBM Research Zurich (Govind Kaigala)

Delivery of minimally dispersed liquid interfaces for sequential surface chemistry

The authors demonstrate rapid liquid switching on a microfluidic probe, which enables localized multi-step surface reactions. The method is implemented using a vertical microfluidic probe, allowing contact-free interaction with an open surface. Several applications, including measurements of receptor–ligand reaction kinetics are demonstrated.

As featured in:

See M. Bercovici, G. V. Kaigala *et al.*, *Lab Chip*, 2016, **16**, 3015.

ROYAL SOCIETY OF **CHEMISTRY**

www.rsc.org/loc

Delivery of minimally dispersed liquid interfaces for sequential surface chemistry†

N. Ostromohov,[ab] M. Bercovici*[a] and G. V. Kaigala*[b]

We present a method for sequential delivery of reagents to a reaction site with minimal dispersion of their interfaces. Using segmented flow to encapsulate the reagents as droplets, the dispersion between reagent plugs remains confined in a limited volume, while being transmitted to the reaction surface. In close proximity to the target surface, we use a passive array of microstructures for removal of the oil phase such that the original reagent sequence is reconstructed, and only the aqueous phase reaches the reaction surface. We provide a detailed analysis of the conditions under which the method can be applied and demonstrate maintaining a transition time of 560 ms between reagents transported to a reaction site over a distance of 60 cm. We implemented the method using a vertical microfluidic probe on an open surface, allowing contact-free interaction with biological samples, and demonstrated two examples of assays implemented using the method: measurements of receptor–ligand reaction kinetics and of the fluorescence response of immobilized GFP to local variations in pH. We believe that the method can be useful for studying the dynamic response of cells and proteins to various stimuli, as well as for highly automated multi-step assays.

Introduction

Delivery of multiple reagents in sequence is central in a large number of surface biochemical assays. For example, protein interactions and function analysis,[1–3] cell stimulation response, signaling and chemical communication studies,[4,5] and nucleic acid hybridization and immuno-assays[6–8] all require delivery of multiple reagents to a reaction site in a fixed order. Manual sequential delivery of reagents for multi-step processes on conventional laboratory platforms, such as slides or 96-well plates, is a time-consuming and labor-intensive task. Automation (*e.g. via* pipetting robots) has enabled the wide-spread use of such assays, particularly in clinical laboratories, where high throughput is required.[9] Increasingly, microfluidic platforms are used for such applications, as they enable the use of small sample volumes, allow individual addressing of a higher density of reaction sites, and provide relatively simple mechanisms for automation and control.[10,11]

In microfluidic devices, the mechanical process of switching between one liquid and another can be performed either off- or on-chip. Off-chip switching can be performed using multiple-position selection valves,[12] solenoid valves,[13]

electromagnetic valves,[14] or pressure controllers,[15] and benefits from the relatively high reliability of these instruments, while maintaining simple fabrication of the microfluidic layer as it does not need to include on-chip moving parts. However, a major practical limitation of such systems is that the physical distance between the switching element and the microfluidic device results in a significant dispersion of the interfaces between reagents, leading to the creation of mixed zones and thus very long transition times. In contrast, on-chip switching[16–20] is able to eliminate much of the dispersion by acting on the liquid in close proximity to the reaction site, but requires complex and expensive fabrication of the microfluidic device, suffers from low reliability, and often limits the range of chemical solutions that can be processed. One strategy for on-chip liquid switching employs capillary pumps,[21,22] which allow autonomous and passive delivery with accurate control of the sequence of the injected liquids and their flow rates, eliminating the need for actuators. However, capillary pumps require the design of a specific dedicated geometry for each assay, and cannot be programmed or adapted in real time. Another strategy for on-chip switching of liquids is integrating micro-mechanical elements such as membrane-valves actuated by pressure.[23,24] These valves allow active and flexible switching of the flow, but require multilayer soft-lithography and the use of externally controlled pneumatic lines.

An elegant solution to this challenge is segmented flow, in which the homogeneous stream of reagent is converted into

[a] Faculty of Mechanical Engineering, Technion – Israel Institute of Technology, Haifa 3200003, Israel. E-mail: mberco@technion.ac.il
[b] IBM Research—Zurich, Saeumerstrasse 4, CH-8803 Rueschlikon, Switzerland. E-mail: gov@zurich.ibm.com
† Electronic supplementary information (ESI) available. See DOI: 10.1039/c6lc00473c

a series of discrete plugs carried by an immiscible fluid, thus confining the interface between liquids and preventing axial dispersion. This principle is most commonly used in segmented-flow analysis and droplet microfluidics for discretization of reactions, enabling multiple tests to be performed in parallel.[25–30] Chin et al.[31] used air segmentation to prevent dispersion between reagents delivered to a reaction site to perform sequential chemistry. This approach is useful for a wide range of assays; however it is not suitable for biological samples, such as live cells which must be kept in aqueous environments to maintain their native properties.[32] This requirement was addressed by Chen et al.,[33] who brought two inclined hydrophobic channels in contact with a hydrophilic surface and used water-in-oil droplets to deliver reagents to the surface. In this method, while the oil was not removed, the sample was still maintained in a purely aqueous environment by utilizing a wetting layer on the hydrophilic surface, which was continuously altered by the incoming droplets. This device allows very rapid sample switching, but operates only on a single reaction site, and requires a conformal physical contact with the substrate.

Here we present a method which allows contact-free sequential delivery of reagents to a reaction surface, with a characteristic switching time of less than 1 s. We use a standard off-chip selection valve to switch between reagents, which are immediately encapsulated as droplets in an immiscible liquid. The droplets confine the dispersion between reagent interfaces, and are delivered to a vertical microfluidic probe (vMFP)[34] – a non-contact scanning device that hydrodynamically confines liquids to a nanoliter-scale volume between an injection and an aspiration channel at its apex. This confined flow can be brought into contact with any surface to drive a reaction. In close proximity to the apex, we implemented a passive phase-separation microstructure that allows complete removal of the oil phase, such that only the aqueous phase exits the chip and reaches the reaction surface. In contrast to previous solutions utilizing segmented flow to deliver processing liquids to a reaction site, implementing this strategy together with complete removal of the oil-phase enables operation without any physical contact between the delivery channels and the surface. The contact-free operation of the MFP prevents perturbation of the sample on the surface and allows addressing multiple reaction sites on the surface automatically. In the Theory section, we provide an analysis of the conditions under which the method can be applied as well as engineering guidelines for the design of such devices. In the Results and discussion section, we characterize the switching time between reagents, and demonstrate two examples of assays that can be implemented using the method: measurements of reaction kinetics and protein response to chemical stimuli. Although our focus here is on open-surface and contact-free analysis, we note that the method is equally applicable to reactions in more traditional closed microchannels.

Experimental

Microfluidic devices

We fabricated the two-layer silicon-glass MFP heads using standard photolithographic and dry-etching techniques, as described previously.[34] The geometry of the MFP channels is provided in Fig. S1 in the ESI.† After fabrication, we coated the channels with a hydrophobic layer by first flowing through the channels piranha solution consisting of sulfuric acid (MicroChemicals GmbH, Ulm, Germany) and 30% hydrogen peroxide (MicroChemicals GmbH, Ulm, Germany), in a ratio of 1 : 3 for 5 min, followed by rinsing with deionized (DI) water (Merck-Millipore, Darmstadt, Germany), and finally flushing the channels with a solution of 50 mM trichloro(octadecyl)silane (Sigma-Aldrich, St. Louis, MO) in hexadecane (Sigma-Aldrich, St. Louis, MO) for 1 min. The piranha solution activates the channel surfaces by introducing hydroxyl groups which covalently bind to the silane molecules, resulting in a hydrophobic surface.[35] Following the hydrophobic treatment of the channels, we dipped the MFP apex in piranha solution for 2 min to ensure that the surface that is in contact with the aqueous immersion liquid is hydrophilic.

Experimental setup

We performed all experiments using an inverted microscope equipped with an automated XY stage (Ti-E, Nikon Instruments, Melville, NY) and an LED white light source (Sola, Lumencor, Beaverton, OR), using a pressure regulator (MFCS-EZ, Fluigent, Villejuif, France) connected to a selector valve (ESS M-switch, Fluigent, Villejuif, France). We used a PEEK T-junction (VICI, Schenkon, Switzerland) with a circular cross section, located at a distance of 1 cm from the selector valve for generation of segmented flow. The flow rates of the aqueous phase and the oil phase were 5 μL min⁻¹ and 4 μL min⁻¹, respectively. The length of the capillary between the selector valve and the MFP head was 60 cm, with a diameter of 125 μm (see Fig. S1 in the ESI† for detailed dimensions). We used a motorized Z-stage (T-LSM050, Zaber Technologies, Vancouver, Canada) to control the distance of the MFP device from the surface. We used MATLAB (R2013a, Mathworks, Natick, MA) to control the selector valve and synchronize it with the light source. For fluorescence experiments, we used a Zyla 5.5 sCMOS camera (Andor Technology, Belfast, NIR, UK), a FITC filter-cube (F36-525, AHF Analysetechnik, Tübingen, Germany) and a 20× water immersion objective (CFI Fluor, NA = 0.5, Nikon Instruments, Melville, NY). For experiments in bright field, we used a Nikon 1 camera (Nikon, Melville, NY) to capture the images. All images were processed and analyzed using MATLAB.

Reagents

In all experiments, we used hexadecane (Sigma-Aldrich, St. Louis, MO) as the organic phase. In the fluorescence switching experiments, the aqueous plugs contained a

concentration of 100 μM fluorescein (Sigma-Aldrich, St. Louis, MO) and DI water. To demonstrate switching between 4 different liquids, we used a 1 : 10 dilution of Amaranth Red (E123), Brilliant Blue FCF (E133), and Dark Green (E104, E133) food dyes (Trawosa AG, St. Gallen, Switzerland) in DI water.

GFP response to pH assay

We immobilized green fluorescent protein (GFP), (Abcam, Cambridge, UK) on an aldehyde-coated slide (SuperAldehyde 2, ArrayIt, Sunnyvale, CA), by depositing 1 μg μL^{-1} of GFP on the surface and incubating it overnight at 4 °C. We rinsed the area with phosphate-buffered saline (PBS) (Gibco pH 7.4, Thermo Fisher Scientific, Waltham, MA) to remove unbound protein molecules from the surface. We used PBS as the immersion liquid, and delivered to the surface a sequence of buffers having pH values between 4 and 9, for 5 s each, and recorded the fluorescence signal of the GFP (for details of the buffer solutions used, see Table S1 in the ESI†).

Association kinetics measurement assay

We prepared a test surface by incubating an aldehyde-coated slide (SuperAldehyde 2, ArrayIt, Sunnyvale, CA) with 100 μg mL^{-1} of rabbit IgG solution (Sigma-Aldrich, St. Louis, MO) at room temperature for 30 min. We rinsed the surface three times using PBS for 2 min, then blocked the surface using 1% BSA in PBS for 30 min, and rinsed the surface again with PBS. We used PBS as the immersion liquid and alternately delivered rhodamine-conjugated anti-rabbit IgG produced in goat (Sigma-Aldrich, St. Louis, MO) and PBS to the surface for 5 s each. To prevent continuous photobleaching of the bound antibodies, we illuminated the surface for 1 s during the delivery of PBS and recorded the signal on the surface. We measured the signal for antibody concentrations of 200 nM, 330 nM and 670 nM.

Theory and principle of the method

Limited switching rate in single phase flow

Consider a sequence of miscible liquid plugs consecutively injected under an external pressure gradient into a channel of length L and a characteristic cross-section length scale a, at a constant cross-section average velocity, U. We assume ideal switching, resulting in an initially sharp interface between each of the plugs. As illustrated in Fig. 1a, the width of this interface increases over time. For a plug containing species with a molecular diffusion coefficient D, the characteristic times of cross-channel diffusion and axial convection can be defined as $t_d = h^2/D$ and $t_c = L/U$, respectively. For $t_c > t_d$, the dispersion of the interface over time is a result of a combination of the axial convection and the transverse diffusion of the parabolic flow-profile, in accordance with the Taylor–Aris dispersion theory.[36] The cross-sectional averaged concentration of species within a plug (in a coordinate system moving at the average flow velocity), c, is then given by[37]
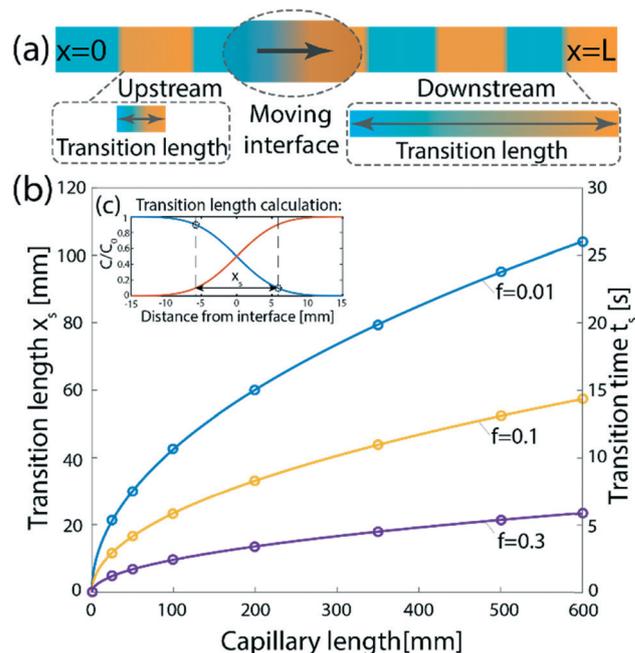

Fig. 1 Dispersion of an initially sharp interface between two plugs injected into a channel under a pressure-driven flow. (a) Schematic illustration of the problem. The interfaces between individual plugs sequentially injected into a channel cannot remain sharp, due to molecular diffusion and the non-uniform cross-section velocity acting to disperse the interface. (b) Theoretical results showing the transition length, x_s (left y-axis), and the transition time (right y-axis), as a function of the capillary length for different values of f. Here, $D = 5 \times 10^{-10}$ m^2 s^{-1}, $U = 4$ mm s^{-1}, $a = 50$ μm, and we assume a cylindrical capillary ($\beta = 1/48$). (c) The transition length is calculated as the distance required for a drop in concentration from $c = (1 - f) \cdot c_0$ to $c = f \cdot c_0$.

$$\frac{\partial c}{\partial t} + \frac{\partial}{\partial x}\left(D_{\text{eff}} \frac{\partial c}{\partial x} \right) = 0$$
$$D_{\text{eff}} = D\left(1 + \beta \frac{U^2 a^2}{D^2} \right),$$

$$(1)$$

where x is the axial coordinate, D_{eff} is the effective diffusion coefficient of the species of interest, and β is a dispersion coefficient that depends on the geometry of the channel. For an initial condition $c(t = 0, x) = c_0 H(x)$, the solution to eqn (1) is

$c(x,t) = \frac{c_0}{2}\left[1 + \text{erf}\left(x / 2\sqrt{D_{\text{eff}} t} \right) \right].$[36,37] As illustrated in Fig. 1c, to assess the extent of mixing between two adjacent plugs at the end of the channel, we define a factor f, which is a measure of dilution of the initial concentration (ranging between 0 and 1), and seek the distance x_s over which the concentration varies from $c = f \cdot c_0$ to $c = (1 - f) \cdot c_0$ at $t = L/U$ (e.g., for $f = 0.1$, this would indicate a variation in concentration between 10% and 90% of the injected concentration). Solving for x on both sides of the interface, with $c = f \cdot c_0$ and to $c = (1 - f) \cdot c_0$, and summing the results to obtain the total transition length, with an effective Péclet number defined as $\text{Pe}_{\text{eff}} \triangleq UL/D_{\text{eff}}$, we obtain

$$\frac{x_s}{L} = \frac{4}{\sqrt{\mathrm{Pe_{eff}}}} \mathrm{erf}^{-1}(1 - 2f). \tag{2}$$

We define the switching time as the time over which the transition length x_s transverses a point at a distance L,

$$t_s = x_s/U \tag{3}$$

Fig. 1b presents the transition length, x_s, and the transition time, t_s, as a function of the length of the capillary, L, for typical values of our setup ($D = 5 \times 10^{-10}$ m^2 s^{-1}, $U = 4$ mm s^{-1}, and $a = 50$ μm). For $f = 0.1$, a 60 cm long capillary (as in the case of our setup) results in a transition time of approximately 15 s, and illustrates the need to limit dispersion.

Principle of the method

To minimize dispersion, we encapsulate the aqueous solution into droplets (discrete phase) in an immiscible organic solvent (continuous phase) in close proximity to the outlet of the selector valve. Thus, mixing between sequentially injected plugs is confined to a single droplet containing the interface, as illustrated in Fig. 2b. We use a phase-separation device located at the end of the channel to remove the continuous phase and deliver only the aqueous plugs to the desired reaction site. The phase separator consists of an array of pillars forming N short capillaries, which are subjected to a negative pressure and, owing to differences in the hydrophobicity of each phase, allow removal of only the continuous phase (see Fig. 3a–c). We implement the method using the MFP to deliver sequences of processing liquids for reaction on the surface, as illustrated in Fig. 2c.

Design considerations

Segmenting the fluid into individual droplets prevents dispersion on a scale larger than the droplet length L_d. However, within the droplet, one can assume near complete mixing.[38,39] Thus, implementing sufficiently short droplets (shorter than the length of the intended transition length) is essential for minimizing the total dispersion. The remaining contributions to dispersion would be the channel segments connecting the valve and the droplet generator, along the phase separator itself, and from the phase separator to the desired delivery site. The total dispersion is thus on the order of

$$x_s \sim O\left(L_d + \frac{4L_P}{\sqrt{\mathrm{Pe_{eff}}}}\right), \tag{4}$$

where L_d is the length of the droplet, and L_P is the length of the channel over which the sample experiences Poiseuille flow. The switching time remains x_s/U.

For a given aqueous flow rate, the size of the individual droplets can be reduced by increasing the flow rate of the organic phase. The maximum flow rate of the organic phase the separator is capable of removing is determined by the number of capillaries formed between the pillars, N, the hydrodynamic resistances of the separator geometry, $R_{h,sep}$, and the additional fluidic path after the separator, $R_{h,add}$. The hydrodynamic resistances can be calculated using the Hagen–Poiseuille equation,[40] and the maximum removed flow rate is given by

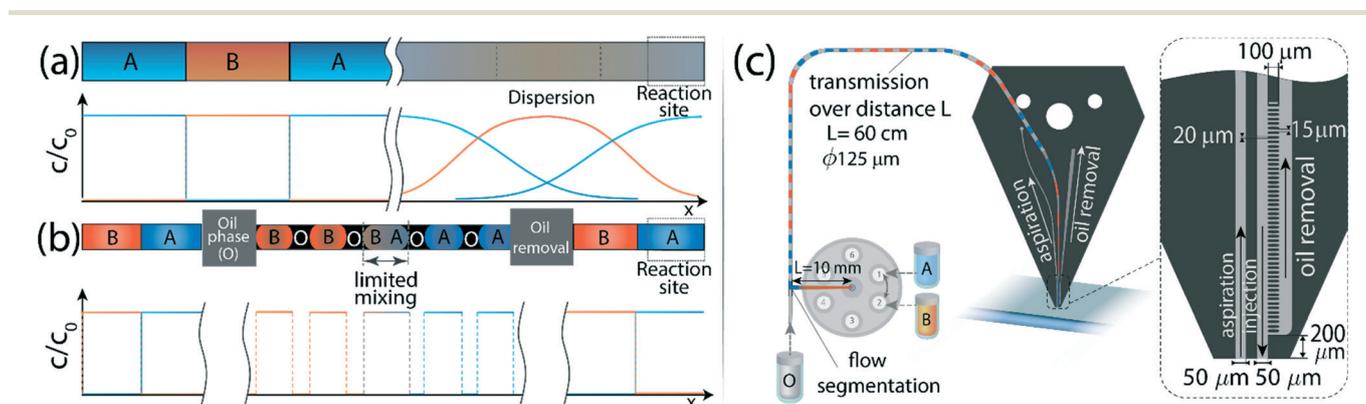$$Q_{max} = \frac{N \cdot \Delta P}{R_{h,sep} + R_{h,add}}, \tag{5}$$

Fig. 2 Schematic illustration of the operation principle which allows sharp interfaces to be maintained between individual plugs over long distances. (a) A train of consecutive liquids has to be delivered to a remote reaction site with minimal cross-contamination between the sections. However, dispersion results in significant mixing between the plugs and loss of the original structure. (b) By encapsulating the aqueous phase into water-in-oil droplets whose length scale is significantly smaller than that of the plug, we limit the dispersion to each droplet. The continuous oil phase is removed in close proximity to the reaction site, allowing only the aqueous phase to continue to the surface while preserving the sharp interfaces between the sections. (c) Implementation of the method on the MFP and description of the setup and channel geometry. Different processing liquids are switched using a selector valve, and are encapsulated in oil using a standard T-junction located at a distance of 1 cm downstream. The droplets are transmitted through a 60 cm long circular capillary, with a 125 μm diameter, to the MFP head where the oil is removed in close proximity to its apex, such that only the aqueous phase reaches the reaction surface. The channels and microstructure on the MFP chip are 50 μm deep. The injection channel has a circular inlet with a 125 μm diameter and is connected to the capillary and sealed using a standard circular dolomite connector (not shown). The width of the injection and aspiration channels at the apex is 50 μm. The oil removal microstructure consists of an array of 20 μm wide and 100 μm long pillars, at a distance of 15 μm from each other, forming 50 rectangular capillaries.
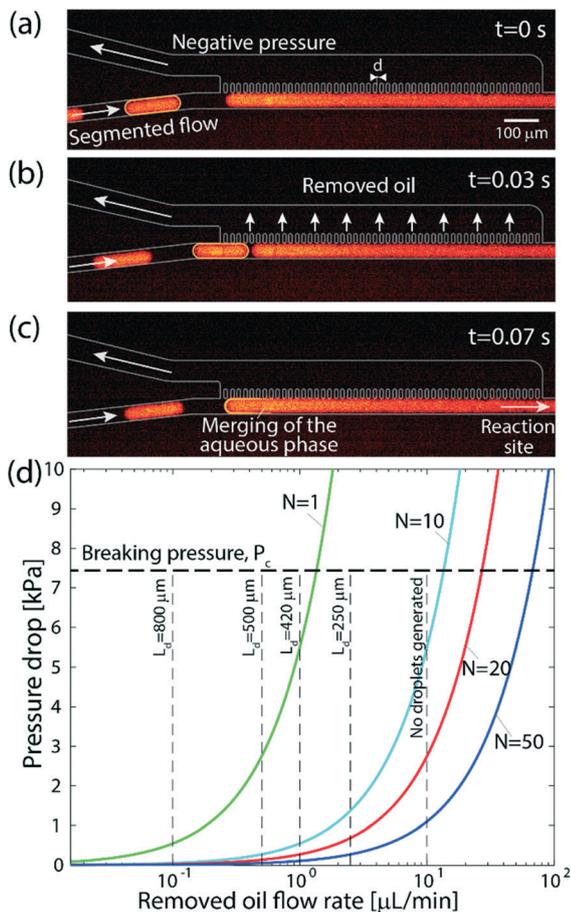
Fig. 3 Operation of the on-chip continuous-phase removal module. (a–c) Sequence of raw fluorescence images showing the operation of the phase-separation structure. (a) The aqueous phase is delivered in individual droplets encapsulated in an organic solvent to an array of 20 μm wide and 100 μm long posts, located at a distance of 15 μm from one another. Across the array, we apply a negative pressure that is sufficiently high to remove the continuous phase, but lower than the capillary pressure of the interface between the phases such that the aqueous phase remains in the main channel. (b) As the oil phase is removed through the array of pillars, the distance between the approaching droplet and the continuous aqueous phase along the pillar array decreases. (c) The approaching aqueous droplet merges and continues through the main channel to the reaction site. (d) Theoretical results showing the maximum continuous phase flow rate that can be removed by the array as a function of the applied pressure drop, and for different numbers of capillaries. As the number of capillaries, N, increases, the device can be operated at higher flow rates and using a lower pressure. The horizontal dashed line represents the capillary pressure, above which the aqueous phase will begin to leak into the removal channel (eqn (6)) calculated for $\gamma = 53.3$ mN m^{-1}. The vertical dashed lines correspond to different droplet lengths obtained experimentally at each of the oil flow rates, for a fixed aqueous phase flow rate of 3 μL min^{-1}. As the mixing is limited to a single droplet, this length affects the transition length after the oil has been removed according to eqn (4). For organic-phase flow rates significantly higher than that of the aqueous phase, no segmented flow can be generated.

where ΔP is the applied pressure drop. The maximum value of ΔP is determined by the capillary pressure in the pillar array.[41,42] The capillary pressure is equal to the product of the interfacial tension between the phases, γ, and the curvature of the surface.[43]

For a rectangular cross section, the principal radii of curvature are half the depth and the width of the capillary, and the capillary pressure in the pillar array is thus given by

$$\Delta P_c = 2\gamma\left(\frac{1}{h}+\frac{1}{d}\right),\qquad(6)$$

where h and d are the depth of the channel and the distance between the pillars, respectively. For a hexadecane–water system, as we use here, the value of the interfacial tension is $\gamma = 53.3$ mN m^{-1}.[44]

Fig. 3 demonstrates the operation of the phase separator and removal of the organic phase from the main channel. As long as the pressure drop across the capillary array is lower than the capillary pressure ΔP_c, the capillary pressure counterbalances the applied pressure drop, preventing the aqueous phase from entering the removal channel, while the organic phase is removed through the array. The removal of the organic phase facilitates the merger of the aqueous droplets into a continuous flow in the main channel, which continues to the desired reaction site. A high frame rate video showing the operation of the phase separator is provided in the ESI† (SM-1).

Fig. 3d presents the maximum flow rate of the organic phase for different separator array sizes and pressure drops. The working point for the desired conditions (appropriate flow rates and minimal dispersion) can be chosen based on eqn (4) and Fig. 3d. For instance, using a geometry consisting of a single capillary, the contribution of the separator to the total dispersion in eqn (4) is negligible, and the mixing length is essentially the length of the droplet. However, oil flow rates higher than 1.3 μL min^{-1} cannot be achieved due to the pressure limitation of ΔP_c, resulting in longer droplets. In contrast, using an array of 20 capillaries allows working at flow rates of up to 26 μL min^{-1}, leading to shorter droplets, but requires a longer separator array, which results in dispersion along the separator.

Results and discussion

Fig. 4 presents a demonstration of flow-switching between two processing liquids delivered to a surface. Fig. 4a presents experimental results of alternately delivering a fluorescent dye (fluorescein) and DI water to the surface, using an oil-removal microstructure with $N = 50$. The signal was analyzed based on an average of a 30×30 μm^2 area in the flow confinement between the channels. The signal on the surface (blue solid line) follows the rectangular input function (orange dashed line), with a switching time of $t_s = 0.56$ s (based on an $f = 0.1$ criterion). The switching time that can be achieved is a function of the flow rate and the length of the segments in which the flow is subject to dispersion, as discussed in the Theory section. For a flow rate of 5 μL min^{-1} and an array of 50 capillaries as we used here, the obtained experimental switching time is comparable with the theoretical value of 0.49 s calculated for dispersion of an interface in
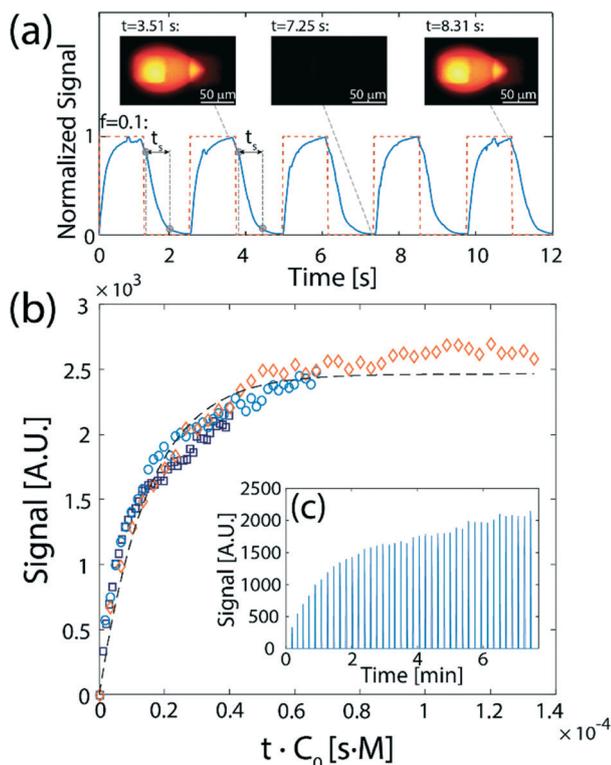
Fig. 4 Demonstration and application of flow-switching between two processing liquids delivered to a surface. (a) Experimental results showing the fluorescence signal resulting from 1.3 s alternating injections of DI and 100 μM fluorescein ($D = 4.25 \times 10^{-10}$ m^2 s^{-1}), traveling a total distance of 60 cm from the valve to the surface. The red dashed line corresponds to the rectangular pulse function actuating the switching valve. The solid blue line shows the average fluorescence in a 30 × 30 μm^2 rectangle located between the injection and aspiration orifices. The resulting switching time of $t_s = 0.56$ s (based on $f = 0.1$) is indicated for the first two cycles. Inset: Raw fluorescence images of the hydrodynamic flow confinement (HFC), viewed from beneath the surface, for three different times along a cycle. (b) Measurement of antibody–antigen association kinetics using flow switching. Alternating 5 s plugs of rhodamine-labeled anti-rabbit IgG ($D = 37 \times 10^{-12}$ m^2 s^{-1}) and of pure PBS are delivered to a surface functionalized with rabbit IgG. Three anti-rabbit IgG concentrations, c_0 were used: 670 nM (diamonds), 330 nM (circles), and 200 nM (squares). All kinetic responses collapse to a single curve as a function of $t \cdot c_0$, resulting in an association constant of $k_{on} = 6.7 \times 10^4$ [M^{-1} s^{-1}]. (c) The signal was analyzed by extracting the peak values recorded during the wash step (pure PBS). In the calculation of the kinetic rate, the time used between measurements is the time over which the surface was exposed to the antibody solution, *i.e.*, 5 s.

the continuous flow sections, 11.7 mm in length. The continuous flow section before the flow segmentation junction, 10 mm in length, causes most of the dispersion, and is responsible for 0.44 s of the total transition time. A video showing the flow-switching between the two liquids is provided in the ESI† (SM-2). The ability to rapidly switch between two liquids, where each maintains a constant concentration in its turn, opens the door to measuring association kinetics using a fluorescently labeled reactant. In Fig. 4b we show the results of experiments in which we switch between an antibody solution containing rhodamine labeled anti-rabbit IgG and pure

PBS buffer, delivered alternately (for a duration of $\Delta t = 5$ s) to a surface with immobilized rabbit IgG. This reaction can be described by Langmuir reaction kinetics,[45,46]

$$c_b = c_s (1 + K_d/c_0)^{-1} \left(1 - e^{-(k_{on}c_0 + k_{off})t}\right) \tag{7}$$

where c_0 is the concentration of the antibodies, c_s is the concentration of the antigen on the surface, k_{on} and k_{off} are respectively the on- and the off-rate of the reaction, K_d is the dissociation constant, $K_d = k_{off}/k_{on}$, and t is the reaction time.

The ability to switch between fluorescently labelled antibodies and non-fluorescent buffer enables the measurement of the fluorescence signal on the surface (indicative of the concentration of antibodies reacted with the IgG on the surface) during the buffer wash, as illustrated in Fig. 4c. Assuming $\Delta t \ll 1/k_{off}$ (an assumption which holds well for the majority of antibodies), each data point corresponds to a reaction time which is the total time over which the surface was exposed to the antibody solution (since both the antibody and buffer are injected at equal intervals, Δt, this time is precisely half of the clock time). As shown in Fig. 4c, the measurements of the signal using three different concentrations of antibodies collapse to a single curve as a function of $t \cdot c_0$, fitting the Langmuir model with an association rate of $k_{on} = 6.7 \times 10^4$ [M^{-1} s^{-1}]. This is consistent with the value of $k_{on} = 6.8 \times 10^4$ [M^{-1} s^{-1}] measured by Sun *et al.*[47] for binding of unlabeled F$_{ab}$ fragments of goat anti-rabbit IgG with rabbit IgG targets.

Fig. 5 presents experimental results of application of switching between multiple processing liquids to perform reactions on a surface. Fig. 5a presents a time-dependent plot of the signal on the surface obtained from switching four processing liquids: (a red dye, a green dye, a blue dye, and DI water), for varying time durations between 5 and 15 s, simulating a hypothetical multiple-step assay. We demonstrate the ability to switch and control the duration of each processing liquid injection on the surface, and show the signal stability over long injection times. This allows one to perform more complex chemical modifications to the surface using the method, such as delivery of longer chemical pulses and their temporal modulation, making the method useful for delivering reagents for multi-step reactions with varying time scales such as ELISA,[48] or sandwich hybridization- and immuno-assays.[10,11] A video showing the switching between the four processing liquids is provided in the ESI† (SM-3).

Fig. 5b presents the use of such switching to obtain, in under 30 s, the fluorescence response of GFP to pH, for six data points in the range 4 to 9. Here, we immobilized GFP on a glass surface, and delivered a set of solutions in a decreasing order of pH. As expected the signal on the surface exposed to the buffers decreases with the reduction in pH. The assay is capable of measuring the steady-state response of the GFP to the change in pH. However, because the time-scale of the dynamic response of a GFP molecule is on the order of 100 μs,[49,50] and is shorter than the switching time between buffers using our device, the signal measured on the surface
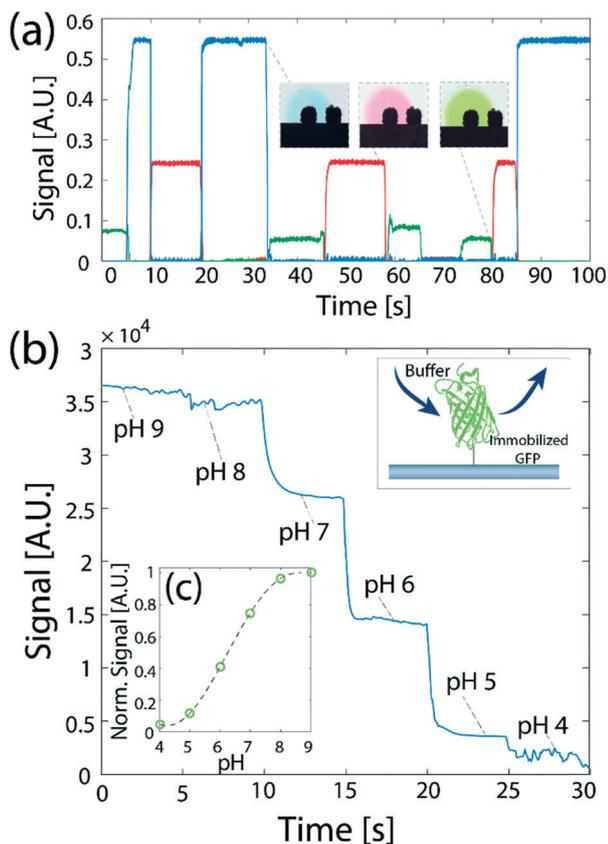
Fig. 5 Demonstration and application of switching between multiple processing liquids to perform reactions on a surface. (a) Demonstration of sequential injection of three different solutions in a desired order. The duration of each liquid injection and the order of the liquids delivered to the reaction site can be accurately controlled. The insets show color images of the flow confinement during the delivery of the different solutions. (b) Switching between multiple liquids is used to study the dynamic response of surface-immobilized GFP to changes in the pH of the buffer. (c) The normalized steady-state signal as a function of pH.

does not capture the dynamic response of the protein to the change in the environmental conditions.

Fig. 5c shows the steady-state signal dependence of the GFP on pH. Our measurements show similar values to previous results by Kneen *et al.*[51] and Haupts *et al.*[50] showing a gradual increase of signal with pH between pH of 5 and 8, with a saturation above a pH of 8 and below a pH of 5. At a pH of 6 the signal increases to 50% of its maximum value (recorded at pH 8–9), and the minimum signal is recorded in the range of pH 4–5 (below 20% of the maximum).

Conclusions

We presented a new method for sequential delivery of reagents to a surface-reaction site, with minimal dispersion of their interfaces. We minimize dispersion by segmenting the (aqueous) flow into individual water-in-oil droplets in close proximity to the switching valve, thus maintaining the dispersion between reagents within small confined volumes. The droplets can then be transported over long distances to the

reaction site. Upstream of the reaction site, we use an array of micro-fabricated pillars, which act as capillaries for removal of the continuous oil phase, thus reassembling the content of the droplets, and allowing only the aqueous phase to come in contact with the reaction site. This makes the method particularly useful for interaction with biological samples, which must be maintained in a well-controlled aqueous environment at all times. We implemented the method on a microfluidic probe designed to deliver reagents to an open surface, and demonstrated two examples of assays which use the method: measurements of receptor–ligand reaction kinetics and measurement of the fluorescence response of immobilized GFP to local variations in pH.

We have demonstrated the application of the method on an open surface using a microfluidic probe fabricated in silicon using standard photolithography and dry etching, but it is important to note that the necessary fabrication resolution would allow straightforward fabrication in other materials such as PDMS, epoxy, or plastic. In fact, the use of a naturally hydrophobic substrate would likely eliminate the need for surface coating which we have used to render the silicon and glass hydrophobic. The method is also equally applicable to sequential delivery of reagents to reaction sites in traditional closed channels.

In the experimental results presented in this work, we used an array of 50 capillaries to ensure that the oil is entirely removed. This resulted in a transition time of 560 ms between reagents (as compared to 15 s when flow segmentation is not used). While for many applications switching times on this order are sufficient, measurements of rapid cellular responses would require a sharper change of environmental conditions, on the order of hundreds of micro-seconds. The switching time in the current implementation of the method is mainly limited by the continuous flow segments between the selector valve and the encapsulation junction, and along the oil-removal micro-structure, where the reagents are subject to dispersion. This limitation may be overcome by replacing the commercially available T-junction and connectors we used here with a customized chip for generation of segmented flow in which the distance to the T-junction will be minimized, and by shortening the oil-removal microstructure (since for lower flow rates merger of the water droplets occurs early along the array). Assuming a negligible distance over which dispersion occurs in the first segment, the optimized switching time that can be achieved is a result of a trade-off between minimizing the length of the oil removal segment and maximizing the flow rates of the reagents. For example, using a flow-rate of 30 μL min^{-1} with 3 functioning capillaries in the array will lead to a switching time of 20 ms. However higher flow rates are not always practical for expensive reagents.

We believe that the method can be particularly useful for studying the dynamic response of biological samples (*e.g.*, cells, proteins) to various stimuli, in which sharp transitions between reagents (*i.e.*, clear initial conditions) are required, as well as for highly automated multi-step assays.

Acknowledgements

References

1 M. Pla-Roca, R. F. Leulmi, S. Tourekhanova, S. Bergeron, V. Laforte, E. Moreau, S. J. C. Gosline, N. Bertos, M. Hallett, M. Park and D. Juncker, *Mol. Cell. Proteomics*, 2012, **11**, M111.011460.

2 S. Darmanis, R. Y. Nong, M. Hammond, J. Gu, A. Alderborn, J. Vänelid, A. Siegbahn, S. Gustafsdottir, O. Ericsson and U. Landegren, *Mol. Cell. Proteomics*, 2010, **9**, 327–335.

3 G. MacBeath, *Nat. Genet.*, 2002, **32**, 526–532.

4 P. Ertl, D. Sticker, V. Charwat, C. Kasper and G. Lepperdinger, *Trends Biotechnol.*, 2014, **32**, 245–253.

5 M. Mrksich, *Curr. Opin. Chem. Biol.*, 2002, **6**, 794–797.

6 X. Pei, B. Zhang, J. Tang, B. Liu, W. Lai and D. Tang, *Anal. Chim. Acta*, 2013, **758**, 1–18.

7 J. Shen, Y. Li, H. Gu, F. Xia and X. Zuo, *Chem. Rev.*, 2014, **114**, 7631–7677.

8 B. Krastins, A. Prakash, D. A. Sarracino, D. Nedelkov, E. E. Niederkofler, U. A. Kiernan, R. Nelson, M. S. Vogelsang, G. Vadali, A. Garces, J. N. Sutton, S. Peterman, G. Byram, B. Darbouret, J. R. Pérusse, N. G. Seidah, B. Coulombe, J. Gobom, E. Portelius, J. Pannee, K. Blennow, V. Kulasingam, L. Couchman, C. Moniz and M. F. Lopez, *Clin. Biochem.*, 2013, **46**, 399–410.

9 G. Wu and S. K. Doberstein, *Drug Discovery Today*, 2006, **11**, 718–724.

10 A. H. C. Ng, U. Uddayasankar and A. R. Wheeler, *Anal. Bioanal. Chem.*, 2010, **397**, 991–1007.

11 L. Wang and P. C. H. Li, *Anal. Chim. Acta*, 2011, **687**, 12–27.

12 J. Ruzicka and G. D. Marshall, *Anal. Chim. Acta*, 1990, **237**, 329–343.

13 K. Ahn and S. Yokota, *Mechatronics*, 2005, **15**, 683–702.

14 X. Liu and S. Li, *J. Lab. Autom.*, 2014, **19**, 444–453.

15 B. Kuczenski, P. R. LeDuc and W. C. Messner, *Lab Chip*, 2007, **7**, 647.

16 K. W. Oh and C. H. Ahn, *J. Micromech. Microeng.*, 2006, **16**, R13–R39.

17 A. K. Au, H. Lai, B. R. Utela and A. Folch, *Micromachines*, 2011, **2**, 179–220.

18 K. Xu, M. R. Begley and J. P. Landers, *Lab Chip*, 2015, **15**, 867–876.

19 A. M. Leach, A. R. Wheeler and R. N. Zare, *Anal. Chem.*, 2003, **75**, 967–972.

20 J. Liu, C. Hansen and S. R. Quake, *Anal. Chem.*, 2003, **75**, 4718–4723.

21 P. Novo, V. Chu and J. P. Conde, *Biosens. Bioelectron.*, 2014, **57**, 284–291.

22 R. Safavieh and D. Juncker, *Lab Chip*, 2013, **13**, 4180.

23 F. Volpetti, J. Garcia-Cordero and S. J. Maerkl, *PLoS One*, 2015, **10**, e0117744.

24 M. A. Unger, H.-P. Chou, T. Thorsen, A. Scherer and S. R. Quake, *Science*, 2000, **288**, 113–116.

25 K. Churski, P. Korczyk and P. Garstecki, *Lab Chip*, 2010, **10**, 816–818.

26 J. Q. Boedicker, L. Li, T. R. Kline and R. F. Ismagilov, *Lab Chip*, 2008, **8**, 1265–1272.

27 B. T. C. Lau, C. A. Baitz, X. P. Dong and C. L. Hansen, *J. Am. Chem. Soc.*, 2007, **129**, 454–455.

28 H. Lange, C. F. Carter, M. D. Hopkin, A. Burke, J. G. Goode, I. R. Baxendale and S. V. Ley, *Chem. Sci.*, 2011, **2**, 765–769.

29 R. A. Kautz, W. K. Goetzinger and B. L. Karger, *J. Comb. Chem.*, 2005, **7**, 14–20.

30 *Advances in flow analysis*, ed. M. Trojanowicz, WILEY-VCH, Weinheim, 2008.

31 C. D. Chin, T. Laksanasopin, Y. K. Cheung, D. Steinmiller, V. Linder, H. Parsa, J. Wang, H. Moore, R. Rouse, G. Umviligihozo, E. Karita, L. Mwambarangwe, S. L. Braunstein, J. van de Wijgert, R. Sahabo, J. E. Justman, W. El-Sadr and S. K. Sia, *Nat. Med.*, 2011, **17**, 1015–1019.

32 H. Yin and D. Marshall, *Curr. Opin. Biotechnol.*, 2012, **23**, 110–119.

33 D. Chen, W. Du, Y. Liu, W. Liu, A. Kuznetsov, F. E. Mendez, L. H. Philipson and R. F. Ismagilov, *Proc. Natl. Acad. Sci. U. S. A.*, 2008, **105**, 16843–16848.

34 G. V. Kaigala, R. D. Lovchik, U. Drechsler and E. Delamarche, *Langmuir*, 2011, **27**, 5686–5693.

35 J. T. Schumacher, A. Grodrian, C. Kremin, M. Hoffmann, J. Metze and J. Micromechanics, *Microengineering*, 2008, **18**, 55019.

36 G. Taylor, *Proc. R. Soc. London, Ser. A*, 1953, **219**, 186–203.

37 R. Aris, *Proc. R. Soc. London, Ser. A*, 1956, **235**, 67–77.

38 J. D. Tice, H. Song, A. D. Lyon and R. F. Ismagilov, *Langmuir*, 2003, **19**, 9127–9133.

39 J. D. Tice, A. D. Lyon and R. F. Ismagilov, *Anal. Chim. Acta*, 2004, **507**, 73–77.

40 L. G. Leal, *Advanced transport phenomena: fluid mechanics and convective transport processes*, Cambridge University Press, 2007.

41 J. G. Kralj, H. R. Sahoo and K. F. Jensen, *Lab Chip*, 2007, **7**, 256–263.

42 A. Günther, M. Jhunjhunwala, M. Thalmann, M. A. Schmidt and K. F. Jensen, *Langmuir*, 2005, **21**, 1547–1555.

43 P.-G. De Gennes, F. Brochard-Wyart and D. Quéré, *Capillarity and wetting phenomena: drops, bubbles, pearls, waves*, Springer Science & Business Media, 2013.

44 G. J. Hirasaki, *J. Adhes. Sci. Technol.*, 1993, **7**, 285–322.

45 I. Langmuir, *J. Am. Chem. Soc.*, 1918, **40**, 1361–1403.

46 P. W. Atkins and J. de Paula, *Atkins' physical chemistry*, W. H. Freeman and Company, New York, 8th edn., 2006.

47 Y. S. Sun, J. P. Landry, Y. Y. Fei, X. D. Zhu, J. T. Luo, X. B. Wang and K. S. Lam, *Langmuir*, 2008, **24**, 13399–13405.

48 J. E. Butler, *J. Immunol.*, 2000, **21**, 165–209.

49 U. Kubitscheck, O. Kückmann, T. Kues and R. Peters, *Biophys. J.*, 2000, **78**, 2170–2179.

50 U. Haupts, S. Maiti, P. Schwille and W. W. Webb, *Proc. Natl. Acad. Sci. U. S. A.*, 1998, **95**, 13573–13578.

51 M. Kneen, J. Farinas, Y. Li and A. Verkman, *Biophys. J.*, 1998, **74**, 1591–1599.